

We are IntechOpen, the world's leading publisher of Open Access books Built by scientists, for scientists

6,900

Open access books available

186,000

International authors and editors

200M

Downloads

Our authors are among the

154

Countries delivered to

TOP 1%

most cited scientists

12.2%

Contributors from top 500 universities



WEB OF SCIENCE™

Selection of our books indexed in the Book Citation Index
in Web of Science™ Core Collection (BKCI)

Interested in publishing with us?
Contact book.department@intechopen.com

Numbers displayed above are based on latest data collected.
For more information visit www.intechopen.com



Aluminium and Its Interlinking Properties

K. Velmanirajan and K. Anuradha

Abstract

Aluminium and its alloys are preferred materials, because of its varied desirable properties, availability and inexpensiveness. Aluminium alloys exist in several different grades available in the market commercially, from pure (about 99% Al content) to specific varieties based on the impurities contained in it by chemical composition. The properties are differing in nature which can be scientifically seen and justified in different perspectives. The properties such as forming, fracture mode, tensile, etc. can be seen through the metallurgical aspect, chemical aspect, crystallographic texture, forming limits and mechanical properties. The truth of its properties can be viewed by interlinking/correlating nature of its different studies. The purpose of this chapter is to show the correlating nature of different properties of aluminium of same and different grades.

Keywords: crystallographic texture, annealing, tensile, formability, void

1. Introduction

Ease of possessing light weight, formability and good strength-to-weight ratio are the desirable properties opted by the designer in the selection of materials for most modern engineering applications. Aluminium alloys vary by their tensile properties, formability properties and surface characteristics from one another at different dimensions, annealing temperatures, duration of annealing and mode of cooling, composition and percentage of initial strain [30–35]. In sheet metal forming, force is applied to a piece of sheet metal to modify its geometry rather than to remove any material. The applied force and stress on the sheet metal beyond its yield strength causes the material to plastically deform, without failing. As a result, the sheet can be bent or stretched into a variety of complex and required shapes. The forming operations of sheet metal include various types and conditions of strains, which can be significantly evaluated to predict the properties of the metal and its forming limit [2]. Preferably, the forming operation is done in most of the engineering applications, which require annealing procedures, microstructure examination, characterization of the sheets and their relations to attain higher formability [3].

The characterization involves the experimental determination of the microstructural aspects, tensile properties and formability parameters such as average plastic strain ratio and planar anisotropy [4]. For evaluating the forming limit diagrams (FLD), the results from the three strain conditions are combined. The formation of the crystallographic texture on the initial material also influences

the formability of the sheet metal. Fracturing occurs in sheet metal forming when the strain exceeds a critical value and is considered as a factor determining the fracture limit diagram. The effect of sheet thickness on formability is a trend in study [5] (Rahavan et al., 2010). It is undertaken to interlink the formability of commercially pure aluminium grades of sheet metal through the study of mechanical (tensile) properties, formability property, forming limit diagrams, void coalescence properties and texture properties by experiments from the established results. Thus the study of the properties by one mode to the other is based on its correlation and interlinking properties.

2. Chemical composition

The aluminium alloy of grades, namely, Al 1350, Al 8011 and Al 1145, available in the market in the form of cold-rolled sheets with different thickness of 1.2, 1.5 and 1.8 mm, respectively, with different chemical compositions are chosen for the study.

Fe and Si particles are capable of stabilizing finer grains, which enhance the strength and ductility [13]. The presence of iron increases the recrystallization temperature, and silicon improves the fluidity of the alloy [25]. The addition of copper reduces pitting corrosion [25]. With the least presence of chromium or manganese and iron, aluminium alloy Al 8011 may form FeAl_3 . The other elements include copper, manganese, magnesium, zinc, chromium, nickel, cadmium, lead and titanium, which are represented in **Table 1** and are in negligible amounts.

Thickness and grade	Remainder Al	Si	Cu	Fe	Sn	Zn	Cr	Mn	Ni	Ti
1.2 mm AA 1350	99.07	0.090	0.139	0.392	0.098	0.010	0.14	0.015	0.019	0.021
1.5 mm AA 8011	98.13	0.919	0.013	0.653	0.096	0.01	0.004	0.026	0.013	0.019
1.8 mm AA 1145	99.4	0.102	0.100	0.254	0.082	0.010	0.003	0.016	0.008	0.025

Table 1.
Chemical composition of commercially pure aluminium alloy sheets of different thicknesses (In wt %) [34, 35].

3. Annealing

Figure 1 indicates the duration of annealing (1hr) which was followed by cooling in furnace. These sheet metals were subjected to four different annealing temperature treatments, namely, 200, 250, 300 and 350°C; soaking time was 1 h, and furnace cooling was considered for experimentation and for forming operations.

4. Microstructure

In a microstructural analysis of Al 1350, the result of the microstructural analysis of Al 1350 has been tabulated in **Table 2**, which has partial recovery and no crystallization at an annealing temperature of 200°C. But at an annealing temperature of 250°C, it has partially recrystallized fully recovered microstructure.

The 200°C annealed sheet shows partial recovery with no recrystallization. The sheet annealed at 250°C is fully recovered and is partially recrystallized

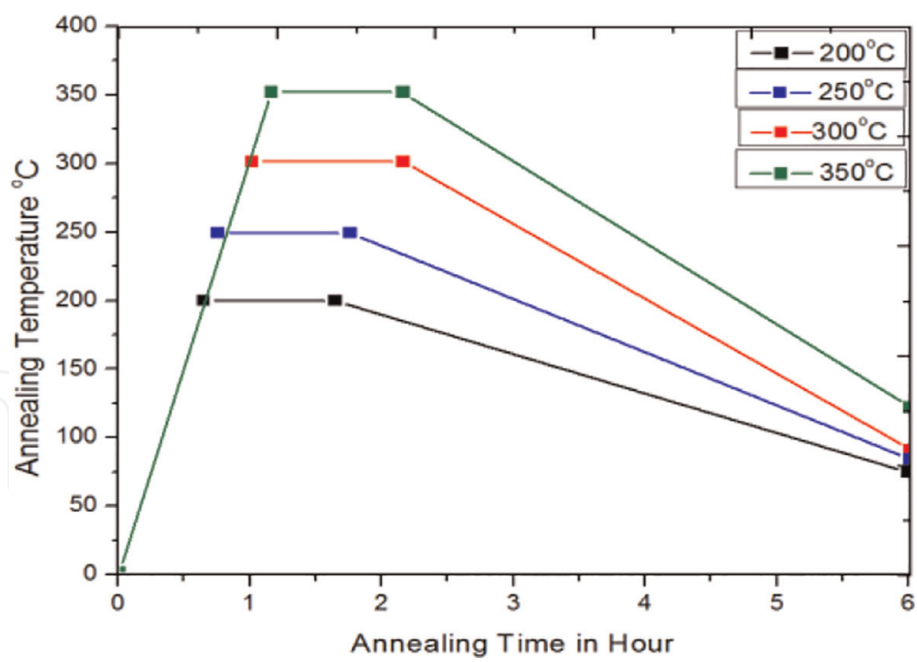


Figure 1.
Diagram showing plot of annealing time versus annealing temperature: (a) 200°C, (b) 250°C, (c) 300°C and (d) 350°C [30, 32–35].

Annealing temperature (°C)	Orientation	n-value	r-value	k-value (MPa)	Yield strength (MPa)	Ultimate strength (MPa)	% elongation
200	0°	0.122	0.583	166.2	119.2	139.9	14.42
	45°	0.144	0.530	171.1			
	90°	0.166	0.521	176.5			
	Average	0.144	0.541	171.2			
250	0°	0.135	0.56	189.4	112.6	129.9	23.58
	45°	0.154	0.692	192.1			
	90°	0.240	0.59	180.8			
	Average	0.171	0.6335	188.6			
300	0°	0.146	0.753	211.3	101.3	116.1	31.10
	45°	0.164	0.602	210.6			
	90°	0.280	0.724	225.4			
	Average	0.189	0.670	214.5			
350	0°	0.167	0.925	290.2	95.6	106.0	45.34
	45°	0.175	0.853	264.14			
	90°	0.290	0.771	280.4			
	Average	0.202	0.851	274.7			

Table 2.
Tensile properties of Al 1350 alloy sheets annealed at different temperatures [30, 32–35].

microstructure, similarly at 300°C also. The sheet annealed at 350°C shows fully recovered and recrystallized microstructure.

The microstructure of the aluminium alloy containing silicon and iron consists of inter metallic phases which appeared as dark areas in the aluminium matrix as shown in **Figure 2**, and certain second-phase particles were found to be present in

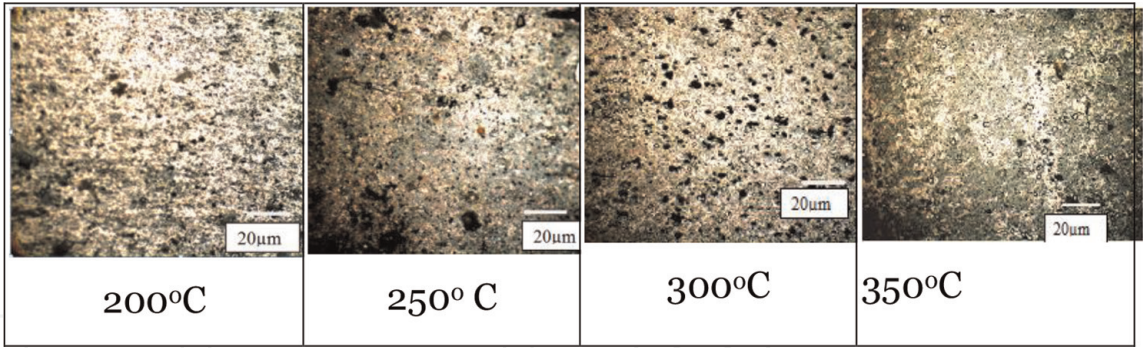


Figure 2. Microstructure of aluminium alloy 1350 sheets annealing at four different temperatures [32, 33].

these alloys. An increase in the annealing temperature shows the presence of a larger amount of precipitated particles; the colour may be grey, which is due to the presence of silicon and white spots [25] is due to the presence of iron, which might ultimately increase the formability. The Fe and Si particles were capable of stabilizing a fine-grain/sub-grain structure, which could be used to develop interesting combinations of strength and ductility [2, 30–35]. Titanium increased the recrystallization temperature, induced grain refinement and remained mostly in solution [26].

5. Mechanical/tensile properties

Ductility and formability could be better indicated by average strain hardening exponent (n_{av}), normal anisotropy value (r_{av}), strain rate sensitivity (m) and $n_{av}r_{av}$ value, and these parameters increased as the annealing temperature increased (Figure 3).

As temperature increased, the $n_{av}r_{av}$ value increased, and formability also increased. The average strength coefficient (K) is comparatively less for the sheet

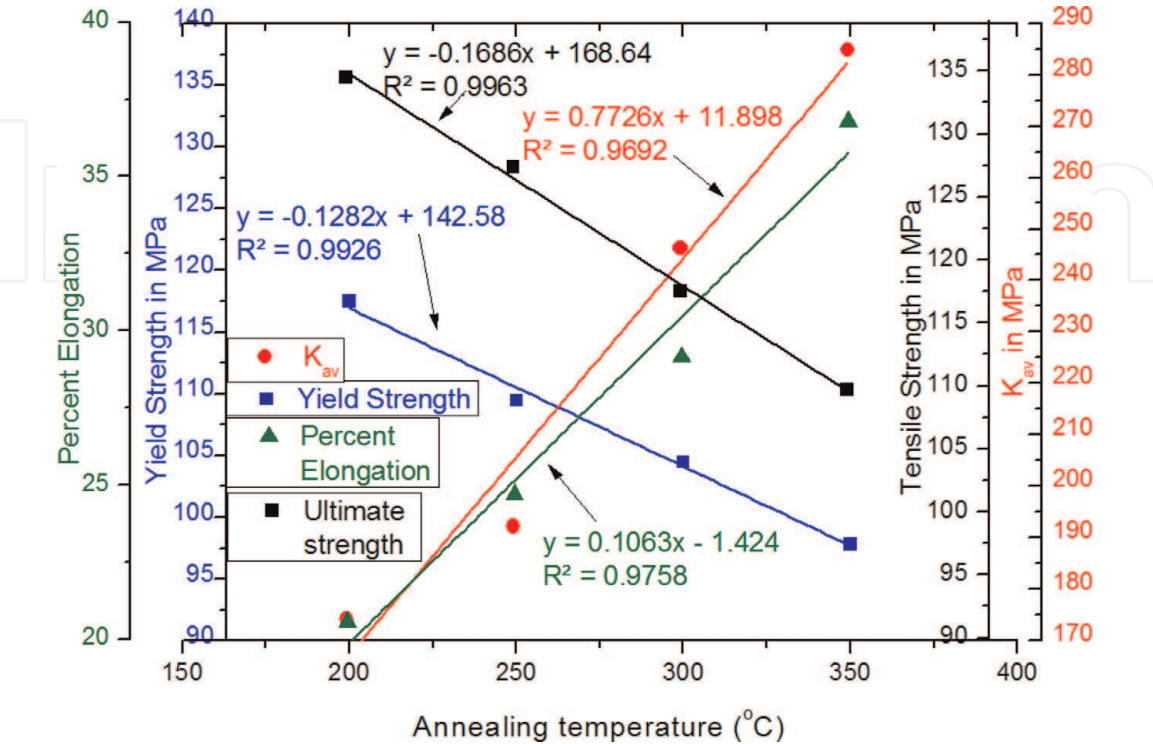


Figure 3. The variation of mechanical/tensile properties with respect to annealing temperatures [30, 32–35].

annealed at 200°C (i.e., low temperature) due to the presence of cold-worked microstructure. At annealing temperatures of 250, 300 and 350°C, the ultimate tensile strength and yield stress of metal sheets were found to be low. The percentage elongation, strain hardening index, anisotropy and k-value, however, increased with annealing temperature. At 350°C, the annealed sheet showed fully recrystallized microstructure, which may be due to relieving of internal strain energy formed during cold working and formation of new strain-free grains which increased the percentage elongation.

This may be due to the softening of metal at higher annealing temperatures. Similar behaviour was observed for all grades of aluminium sheets selected. In Al alloy sheet, the factor $n_{av}r_{av}$ formability index showed a direct relationship with formability of sheet metal. As the factor $n_{av}r_{av}$ increased, the formability also increased [2, 27, 28]. The percentage increase of $n_{av}r_{av}$ index in zone 3 was found to be highest due to fully recrystallized microstructure as shown in **Figure 4**. The next highest was observed in zone 1 (due to full recovery) followed by zone 2. Similar behaviour was observed in all commercially available Al sheets annealed at different temperatures.

Tables 2 and 3 show the different annealing temperatures of aluminium alloy sheet metals with different mechanical properties and formability properties, namely, strain hardening exponent, yield strength, tensile strength, r-value (plastic

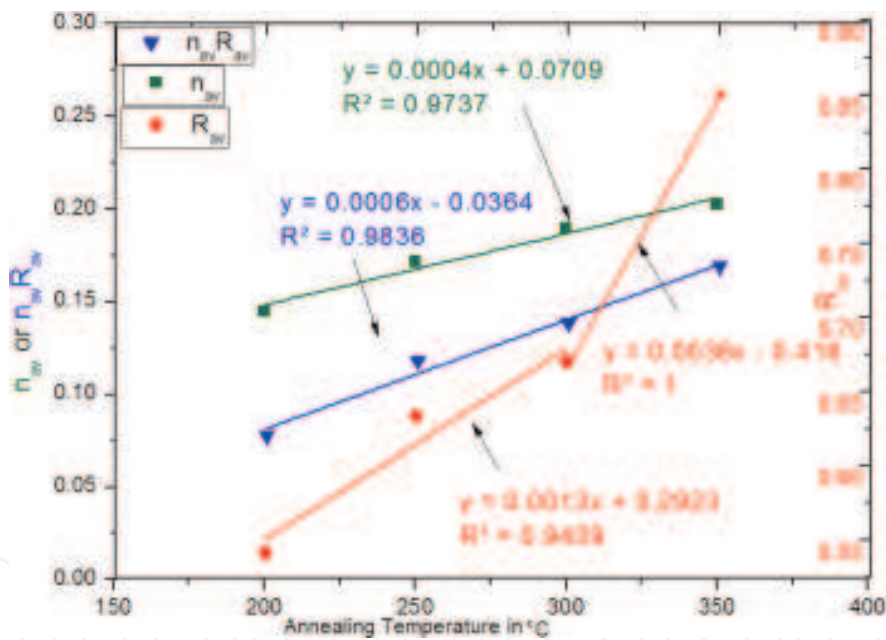


Figure 4.
The variation of formability properties with respect to annealing temperatures.

Annealing temperature (°C)	Orientation	n_{av}	Δr	r_{av}
200	0°	0.071126	0.0220	0.541
	45°	0.07632		
	90°	0.086486		
	Average	0.077563		
250	0°	0.09423	0.0025	0.693
	45°	0.106568		
	90°	0.16584		
	Average	0.118302		

Annealing temperature (°C)	Orientation	nr_{av}	Δr	r_{av}
300	0°	0.10994	0.0005	0.738
	45°	0.12103		
	90°	0.20272		
	Average	0.13868		
350	0°	0.15448	−0.0050	0.851
	45°	0.14928		
	90°	0.22359		
	Average	0.169153		

Table 3.
Formability parameters of Al 1350 alloy sheets annealed at different temperatures.

strain ratio) and percentage elongation, were evaluated in this work. Since the sheet metals were anisotropic in nature, the normal anisotropy parameters such as r_{av} , nr_{av} and Δr were also evaluated.

The n-value and k-value were found to be maximum at 90°C to the rolling direction (RD) and minimum along the RD for the Al 1350 alloy sheet annealed at 200°C. Under similar conditions, the r-value was maximum along the RD and minimum at 90°C; the n-value showed similar observations, whereas the k-value and r-value were maximum at 45° to the RD and minimum at 90° to the RD.

6. Forming properties

6.1 Evaluation of forming limit diagram

Tension-compression, tension-tension and plane strains are the three regions of strain conditions formed due to the variation in the width of the specimen. The forming limit diagram was plotted based on the grid circles from **Figure 5a** and stretched various ellipses from **Figure 5b** with respect to the strain condition as a base.

Using a travelling microscope, the ellipse dimensions like minor and major diameters were measured with an accuracy of 0.01 mm. These measurements of major and minor diameters were used to calculate the major strain (ϵ_1) and the minor strain (ϵ_2). The strains ϵ_1 and ϵ_2 were measured at the safe, neck and fracture

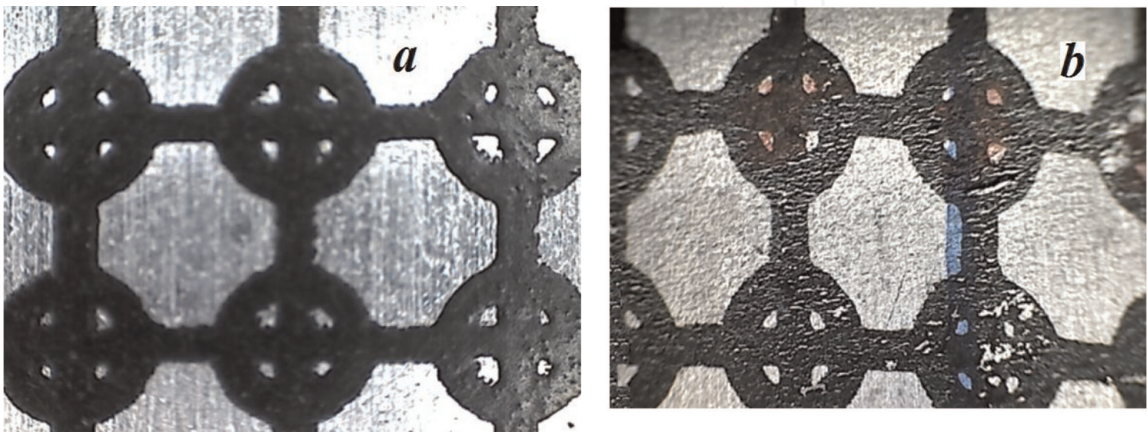


Figure 5.
Chemically etched grid circles (a) before and (b) after the forming process.

Annealing temperature (°C)	Tension-tension strain condition		Plane strain condition	Tension-compression strain condition	
	Major strain	Minor strain	Major strain	Major strain	Minor strain
200	35	18	17	28	−3
250	38	17	21	32	−6
300	43	15	29	38	−13
350	50	13	31	45	−14

Table 4.
Value of limiting strain in percentage for various strain conditions of Al 1350 alloy sheets.

Annealing temperature (°C)	Major strain values in percentage		
	TC region at minor strain −0.075	PS region	TT region at minor strain 0.15
200	109	98	83
250	111	102	85
300	116	108	91
350	125	116	99

Table 5.
The maximum major strain at fracture for Al 1350 alloy sheets.

regions to plot the forming limit diagrams. These strains were measured in three distinct regions like safe region, neck region and fracture region using the formulae natural log of deformed to the original dimension, whereas thickness strain (ϵ_3) was determined at fracture region. The limiting strains and major strains at fracture were calculated for Al alloy sheets from major and minor dimensions at four different annealing temperatures and have been presented in **Table 4**.

The minor and major diameters of ellipse were measured using different mode of strain conditions. They are tension-tension (TT), plane strain (PS) and tension-compression (TC). The grid circles were etched over the shape of the plate and became elliptical with different major and minor diameters based on the strain conditions, which is the input to plot forming limit diagram (**Table 5**).

Studies on ductile material models have been used to investigate the nucleation of voids and void coalescence as well as the interaction between different size and scales of voids [2]. This could be used to predict fracture mechanisms in structural components or test specimens. Ductile crack growth by void coalescence is an application [26]. Hence, fractography and void coalescence properties are analysed in the following sections.

7. Limiting strains

The forming and fracture limit diagrams of various grades of aluminium alloys chosen have been presented in **Figure 7** along with the limiting strains of various grades of aluminium at different annealing temperatures. A minor strain of 19% and major strain of 21% have been recorded at the lowest temperature of 200°C. The major strain of the same sheet at PS condition was 31%. In TC region major and minor strains were found to be 33% and 3% respectively. Due to the presence of cold rolled refined grains in microstructure, poor formability was shown by the

sheet annealed at 200°C. The proportionate increase in formability with the annealing temperature has been confirmed through these experiments.

In tension-tension region, the sheet annealed at 250°C possessed a maximum minor strain of 17% and maximum major strain of 37%. In plane strain condition, the limiting major strain was about 39%. In tension-compression strain condition, the maximum minor and major strains were –7 and 38%, respectively. In tension-tension region, the sheet annealed at 300°C possessed a maximum minor strain of 15% and maximum major strain of 41%. In plane strain condition, the limiting major strain was about 41%. In tension-compression strain condition, the strain values increased as the annealing temperature increased. At an annealing temperature of 350°C TT region, the minor strain was 13% and major strain 51%. The fracture limit minor strain was found to be—17% and limit major strain was 53% in the TC region.

The sheet annealed at 350°C exhibited lower yield stress, higher *n*-value, higher *r*-value and favourable microstructure for its better formability, when compared to the other sheets. These results were in good agreement with the findings of Narayanasamy et al. [1]. The increased value of *n* and *r* for sheet annealed at 350°C showed good stretchability, and it was in agreement with the evaluation carried out using FLD. The tendency for earing was very less during drawing operations due to its very high *r*-value. This was in good agreement with the findings of Ravindran et al. [26].

8. Fractography

The fractured surfaces were studied using scanning electron microscopy (SEM) which revealed the nature of fracture and correlated with formability and its parameters. The fracture zone of formed samples in 10 mm × 10 mm size portion was removed from the fractured specimen, and SEM images were captured from perpendicular face having dimples and voids as a result of fracture. The fractured surfaces were observed using a SEM model LEO 420. The void parameters were recorded from the SEM images through void coalescence studies using CAD 2010 modelling software. Magnifications at 3000, 2000 and 800 X were done using an accelerating voltage of 3×10^4 V and an emission current of 9.1×10^5 nA.

8.1 Void coalescence study

The voids were analysed with respect to perimeter (πd), relative spacing of the ligaments present between the two consecutive voids (δd), length of void (*L*) and width of void (*W*) by using the mouse of the computer. From the perimeter (Tables 6 and 7), the diameter of the voids was determined. In the void parameter, *d*-factor was determined by using the empirical relation arrived by dividing (δd) by the average radii of the voids present in void perimeters. To find the void area fraction, the total area of voids in that particular area (called representative material area) was calculated:

$$d - \text{factor} = \text{ligament thickness} / \text{average radii of the voids} \quad (1)$$

$$\text{Void area fraction} = \text{total area of the voids} / \text{representative material area} \quad (2)$$

SEM images were used to measure the relationship between fracture and formability parameters from the blank shown in Figures 6 and 7.

Annealing temperature (°C)	Average void size in μm for various metal specimens							
	Deep drawing (tension-compression)			Plane strain		Biaxial stretching (tension-tension)		
	60 mm	80 mm	100 mm	120 mm	140 mm	160 mm	180 mm	200 mm
200	7.3	6.19	6.08	5.09	4.51	4.11	3.9	3.7
250	7.8	7.5	6.55	6.1	5.5	5.2	4.8	4.2
300	8.5	8.3	7.9	7.5	7.2	6.751	6.24	5.76
350	10.22	9.92	9.89	9.01	8.5	8.21	8.1	7.99

Table 6.
Average void size found on formed and annealed Al 1350 alloy sheets with different specimen width.

Annealing temperature range	Percentage change in void parameters					
	Region	δd	Void size	d-factor	(L/W) ratio	V_a
200–250°C zone 1	TC	15.96	7.73	−41.90	−40.41	42.67
	PS	13.34	19.84	−32.39	−31.13	19.52
	TT	12.07	23.07	−31.42	−25.05	7.35
250–300°C zone 2	TC	10.22	8.97	−30.99	−20.25	25.51
	PS	10.12	22.95	−24.37	−18.32	18.07
	TT	5.54	29.92	−16.65	−14.56	11.38
300–350°C zone 3	TC	18.85	19.51	−51.70	−24.15	29.10
	PS	30.48	21.61	−52.46	−23.27	24.76
	TT	33.02	38.71	−51.88	−28.49	20.11

Table 7.
Percentage change in void parameters for different annealing temperature ranges.

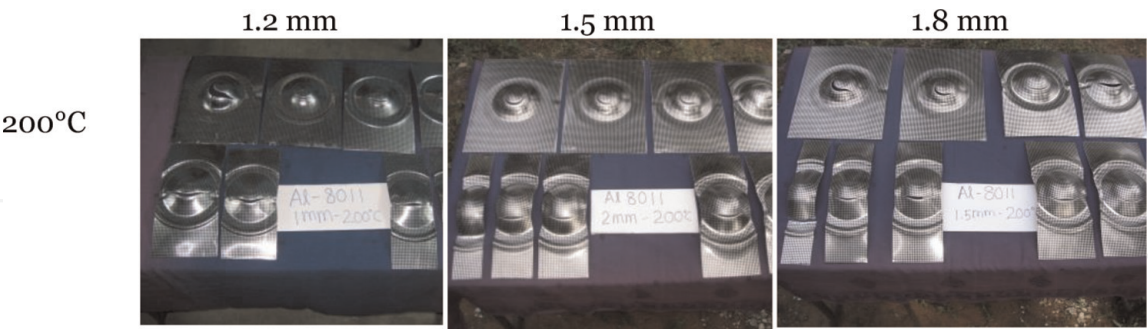


Figure 6.
Cupping test specimens of aluminium alloy of three thicknesses, annealed at different temperatures (after forming) [30, 32–35].

8.2 Void shape

The shape of the voids and L/W ratio was found to vary with stress/strain ratios. The L/W ratio was high in TT conditions and less in the TC condition. The prolate voids showed elongation along the thickness region whereas the oblate along the plane of the sheet [29].

8.3 Void size

For the blanks subjected to tension-compression strain condition, the SEM images showed many bigger micro-voids and dimples, and their surface was rough

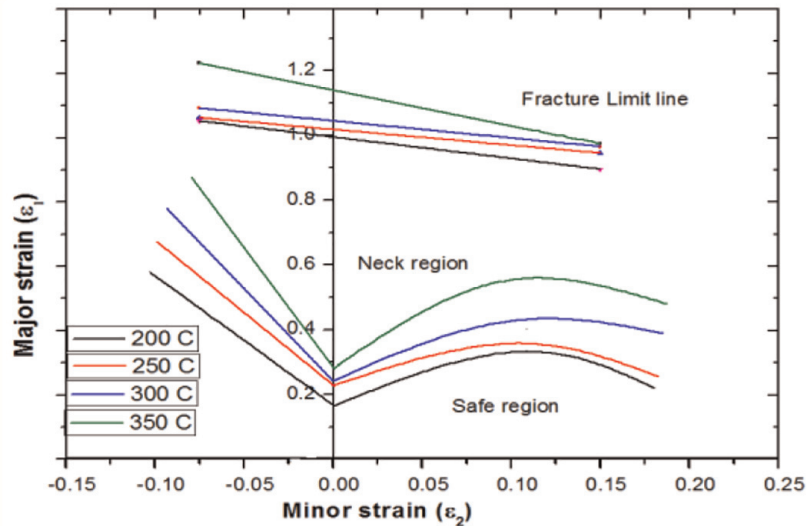


Figure 7.
Forming limit diagram of Al sheet of various grades [34, 35].

and irregular. This showed shear type of fracture with deep dimples [1]. The surface of the metal sample was smooth with shallow dimples and less voids in plain strain condition, whereas in TC condition, the SEM images showed larger voids and deep dimples, and hence the surface was irregular. This indicated the presence of shear type fracture with deep dimples [2]. For the blanks subjected to plane strain condition (blank width of 120 mm), the surface was smooth compared to the tension-compression condition with less number of voids, shallow dimples and less fracture area.

8.4 Void area fraction

The number of voids as well as their type were affected by the forming conditions [1]. The sheets annealed at 350°C showed a larger number of voids and deformation than sheets annealed at 200, 250 and 300°C. This could be due to the presence of fully recrystallized grains. The microstructure also clearly indicated a favourable interaction between precipitation and recrystallization [26] at 350°C. If the strain hardening index (n) value was more, the strain required for the plastic deformation was also more. During annealing at 350°C, the strain hardening index value was high.

8.5 L/W ratio

Length-to-width ratio in the void. The L/W ratio of void for the sheet annealed at 200°C was found to be the highest.

9. Interlinking effects of void parameters

9.1 Effect of void properties with annealing temperatures

Figures 8 and 9 showed the variation of void properties with respect to annealing temperatures in different regions such as (a) TC, (b) PS and (c) TT.

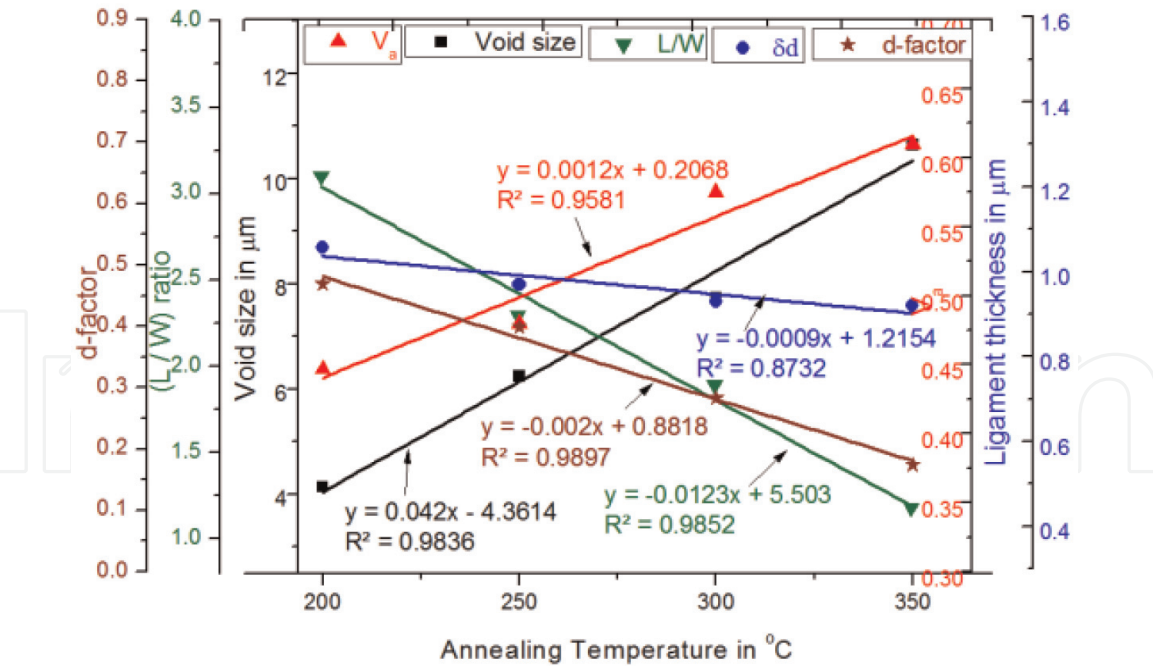


Figure 8.
Variation of void properties in Al 1350 alloy with respect to annealing temperatures in different regions.

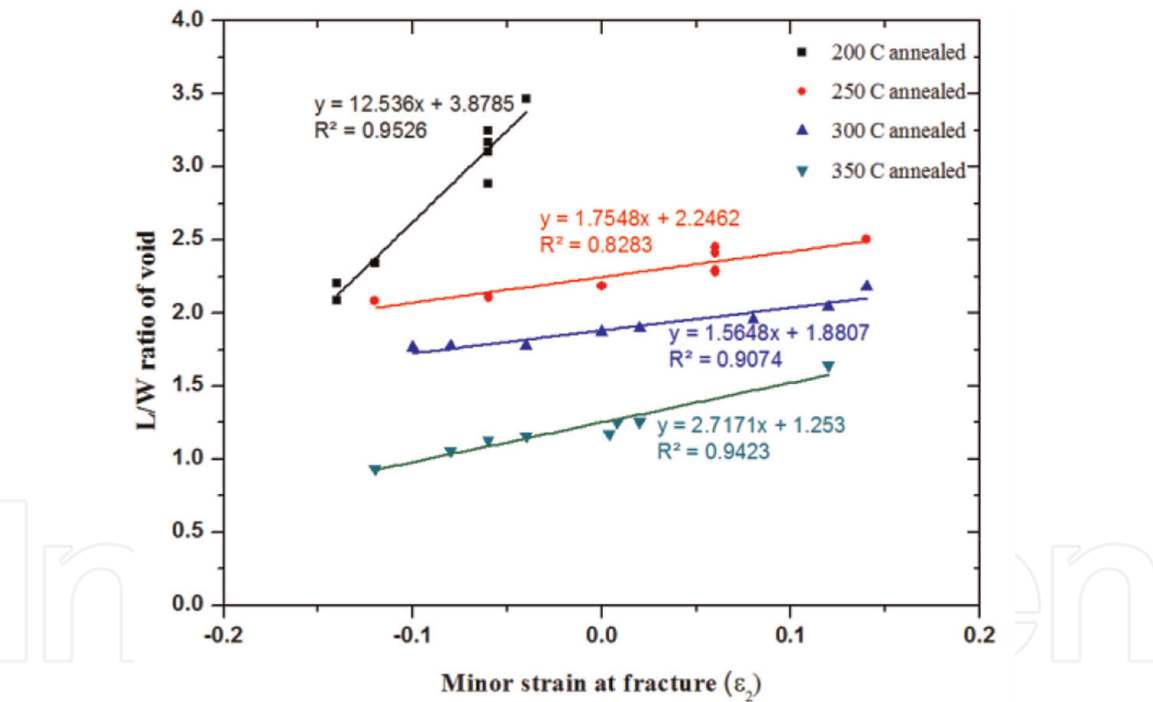


Figure 9.
 L/W ratio of voids vs. minor strain at fracture (ϵ_2) at various annealing temperatures and thickness.

The slope value obtained for void size was high for TC region because they showed more plastic deformation.

This might be due to the fact that one stress was tension and the other was compression which increased the maximum shear stress of the Mohr's circle. The intercept value for void area fraction plot was high for **TC region** compared with **TT region** because in TC region the plastic deformation was higher.

The slope value and the ligament thickness of annealed sheet were found to decrease in the TC region than that in TT region. This might be due to plastic deformation of the metal sheet.

9.2 Effect of L/W with minor strain

9.3 Effect of void area with minor strain

Figure 10 shows a plot between void area fraction and the mean strain for all sheets which have been tested. As observed from the figure, the void area fraction for the sheet annealed at 200°C has been found to be the lowest of all sheets tested.

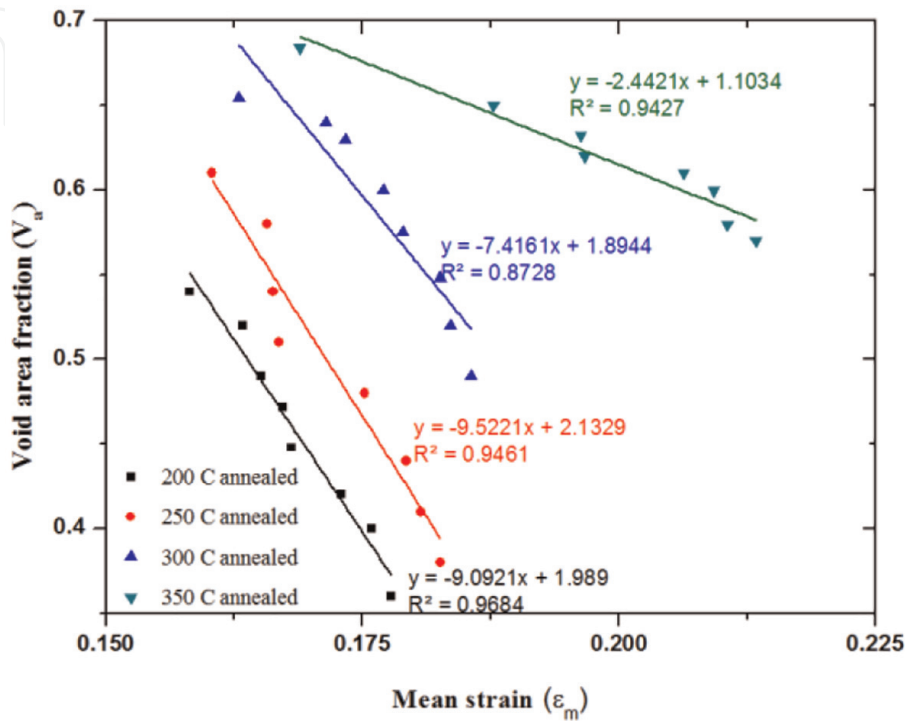


Figure 10.
Void area fraction (V_a) vs. mean strain (ϵ_m) at various annealing temperatures.

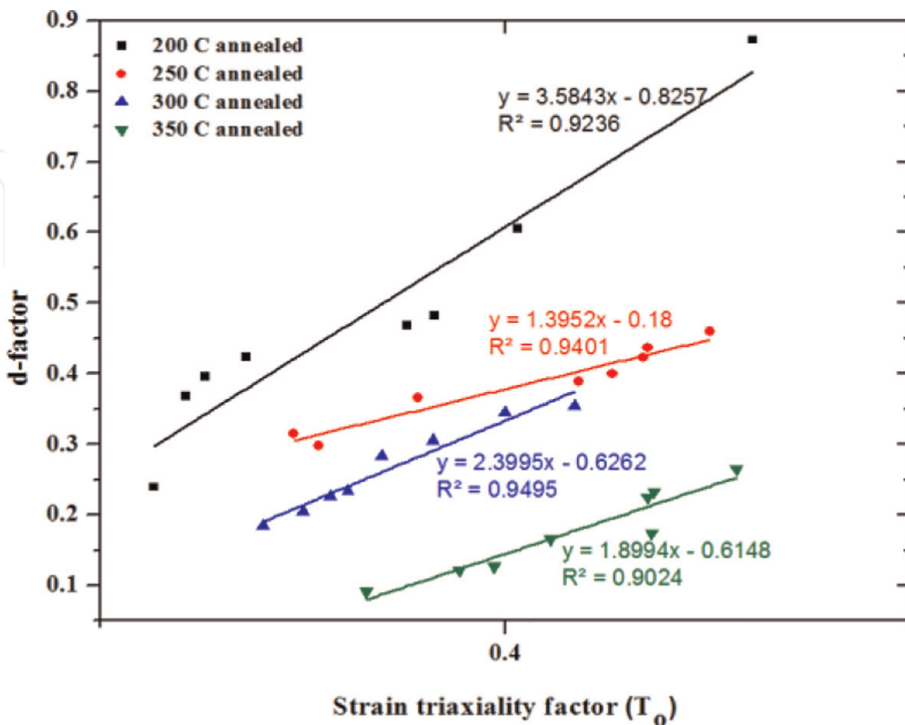


Figure 11.
 d -factor vs. strain triaxiality factor (T_o) at various annealing temperatures.

9.4 Effect of d-factor with strain triaxiality ratio

Figure 11 shows a plot between d-factor and strain triaxiality ratio for all sheets tested. As the strain triaxiality ratio increase, the d-factor also increased. As the d-factor increased, the formability of the sheet decreased and vice versa.

The d-factor was found to be lowest for the metal sheet annealed at 350°C indicating formability property compared to the sheets annealed at different temperatures.

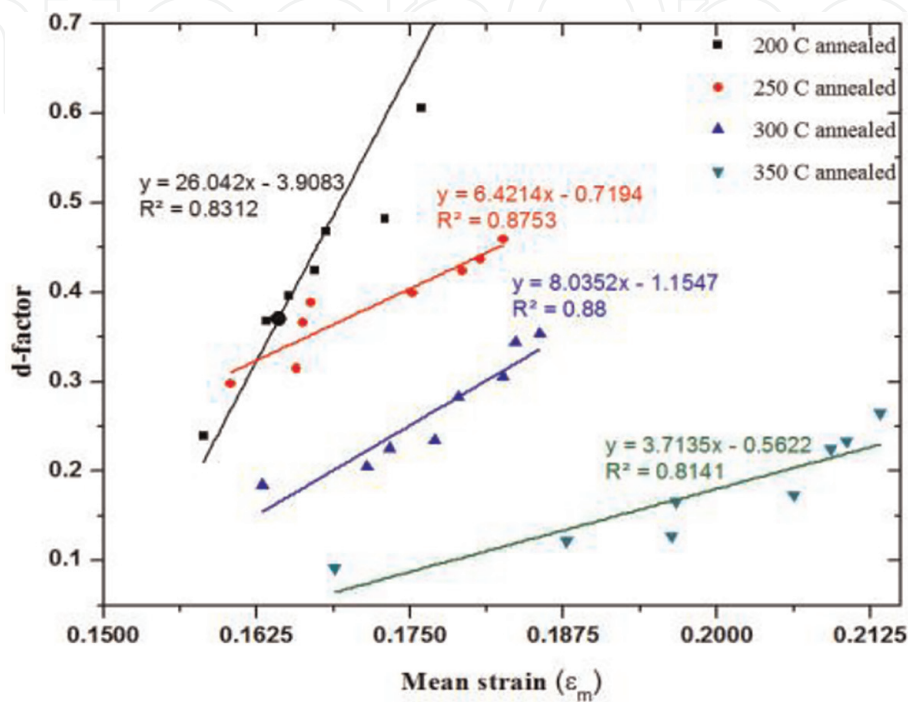


Figure 12.
d-factor vs. mean strain (ϵ_m) at various annealing temperatures.

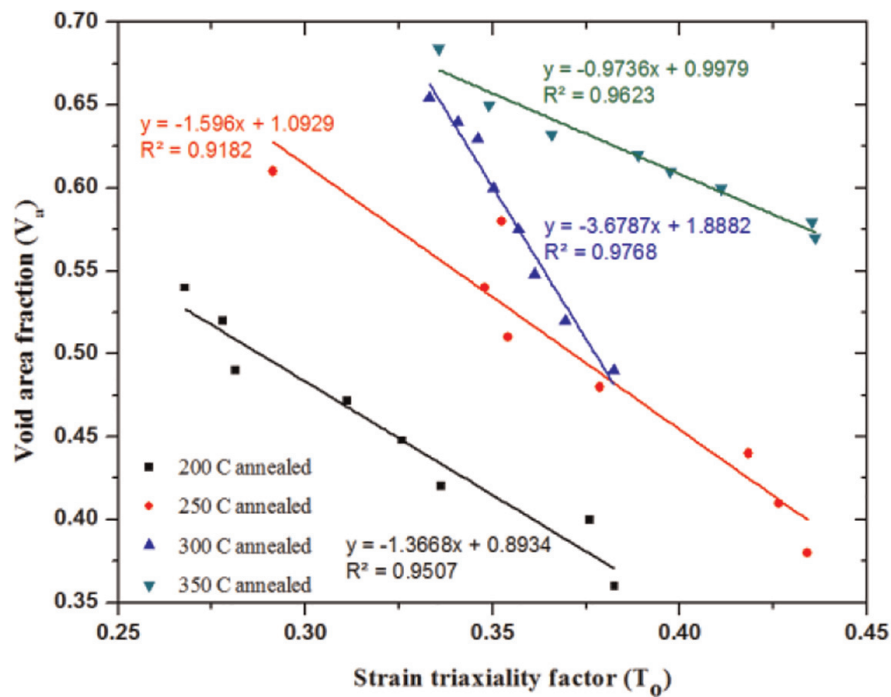


Figure 13.
Void area fraction (V_a) vs. strain triaxiality factor (T_o) at various annealing temperatures.

In the case of sheet annealed at 350°C, the ligament thickness was lowest and exhibited the best formability among the sheets tested. As the stress state moved from tension-compression to tension-tension region, the ligament thickness decreased. Similar behaviour was observed for all grades of aluminium sheets selected. The sheets annealed between these temperature show the corresponding changes recorded in the ligament thickness, which confirms with the prediction of Narayanasamy et al. [2].

9.5 Effect of d-factor with mean strain

The relationship between the hydrostatic/mean strain and the d-factor has been shown in **Figure 12**. The d-factor linearly increase as the hydrostatic strain increases for all sheets tested. Even for a large mean strain developed during forming, the d-factor value was less. The rate of change was in good agreement with the findings of Narayanasamy et al. [1], whereas the d-factor was found to be the highest for sheet annealed at 200°C due to the presence of Si and poor recovery in processing.

9.6 Effect of void area fraction and strain triaxiality ratio

It has been observed that the void size of the sheet annealed at 350°C was approximately 8.21–12.9 μm , whereas for the sheets annealed at 250 and 300°C, the void size was 3–6 μm . The larger void size may be due to good recrystallization, and smaller void size may be due to poor formability at lower annealing temperature. The sheets annealed at 200°C possessed low V_a and sheets annealed at 350°C

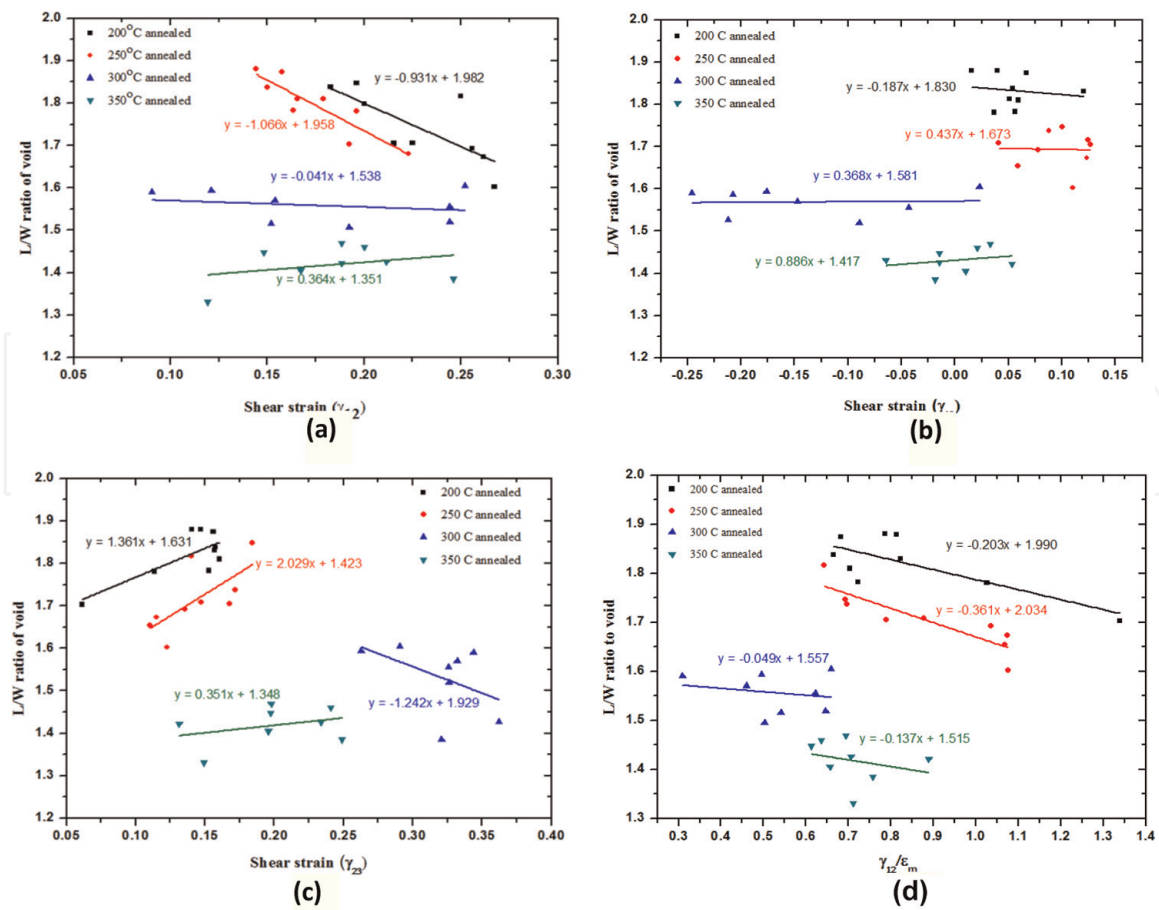


Figure 14. L/W ratio of voids vs. shear strains at various annealing temperatures for Al alloys: (a) γ_{12} , (b) γ_{13} , (c) γ_{23} , (d) γ_{12}/ϵ_m .

showed higher value of V_a (**Figure 13**) which was in close agreement with the findings of Narayanasamy et al. [2].

9.7 Effect of L/W ratio of voids and shear strains

The L/W ratio of voids was correlated with various shear stresses calculated from Mohr’s circle like γ_{12} , γ_{13} , γ_{23} and γ_{12}/ϵ_m at all annealing temperature conditions which has been shown in **Figures 14–16**. For sheets annealed at 350°C, negative sloped curves were obtained due to high L/W ratio, whereas the sheet annealed at

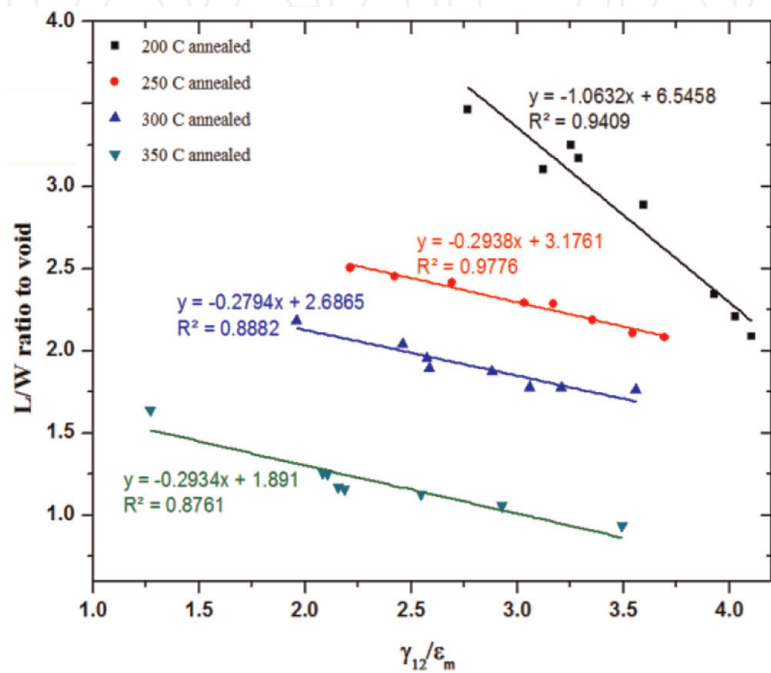


Figure 15.
L/W ratio of void vs. shear strains at various annealing temperatures for Al 1145 alloy.

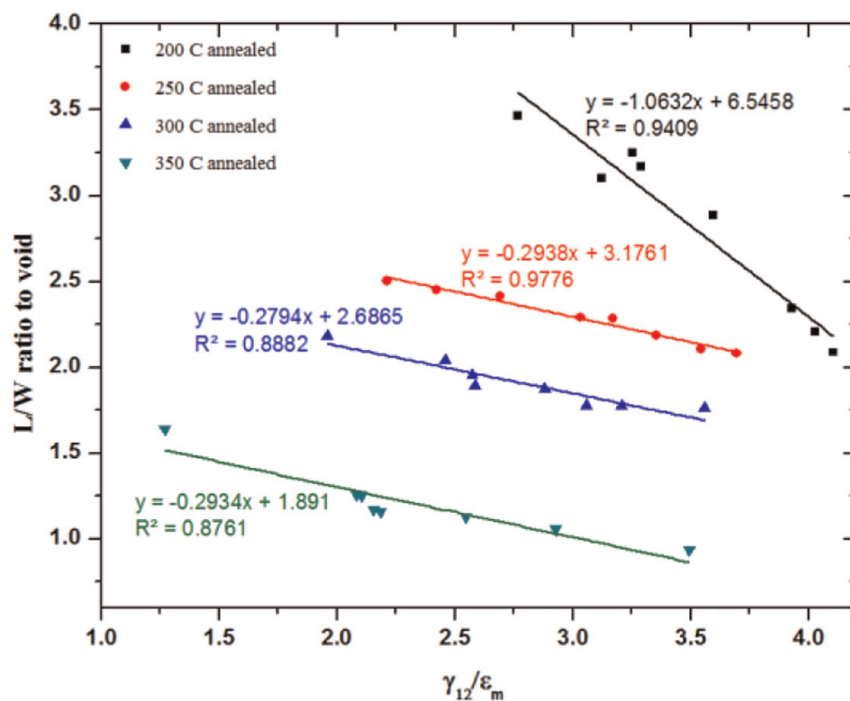


Figure 16.
L/W ratio of void vs. shear strains at various annealing temperatures for Al 1350 alloy.

200°C showed positive sloped curves because of their low L/W ratio. These findings were in good agreement with those of Narayanasamy et al. [1, 26].

10. Crystallographic texture

A crystal is characterized by the periodic arrangement of its elements (atoms, ions) in space. In the field of material science and engineering, the distribution of the crystallographic orientations of a polycrystalline sample is called as texture. If these orientations were fully random in a sample, it had no texture. If the crystallographic orientations have some preferred orientation but were not random, then the sample has different textures, namely, weak, moderate and strong. The crystal having the preferred orientation and its degree was dependent on the percentage [6]. Texture can have a great influence on the material properties and is seen in almost all engineered materials. If all crystallites had the same orientation, the anisotropy of the polycrystal exactly equals that of the single crystal [7]. In an isotropic texture, all orientations occur with the same probability; the behaviour of the polycrystalline material was isotropic even though every single element (crystallite) showed an anisotropic behaviour (Engler et al., 2001).

10.1 Crystallographic texture analysis

Texture can be determined by various methods, namely, quantitative analysis and qualitative analysis. In quantitative techniques, the most widely used is X-ray diffraction using texture goniometry. Often texture has been represented using a pole figure, in a stereographic projection, a specified crystallographic axis (or pole) from each of which a representative number of crystallites which was plotted, along with the directions relevant to the material's processing history. These defined directions are called as a sample reference frames.

10.2 Common textures

The commonly found textures in processed materials are cube $(0\ 0\ 1)\langle 1\ 0\ 0\rangle$, brass $(1\ 1\ 0)\langle -1\ 1\ 2\rangle$, copper $(1\ 1\ 2)\langle 1\ 1\ -1\rangle$ and S $(1\ 2\ 3)\langle 6\ 3\ -4\rangle$ [9]. These were given in miller indices for simplification purposes.

10.3 Orientation distribution function

The ODF is defined as the volume fraction of grains with a certain orientation. The orientation is normally identified using three Euler angles. The orientation distribution function cannot be measured directly by any technique. But it can be state by a sum of functions or expand it in a series of harmonic function [9]. Others, known as discrete methods, divide the ODF space in cells and focus on determining the value of the ODF in each cell.

10.4 Origin

The making of metal sheet often involves compression in one direction and, in efficient rolling operations, tension in another, which can orient crystallites in both axes, by a process known as the grain flow. New crystallites that arise with annealing usually have a different texture [7]. The control of texture was extremely important during the making of a silicon steel sheet for transformer cores (to reduce

magnetic hysteresis) and of aluminium cans (since deep drawing requires extreme and relatively uniform plasticity) [8].

11. Texture properties

Texture significantly affects the formability which is usually evaluated in terms of forming limit diagrams [1]. Although much research has been carried out, their correlations have not yet been completely clarified. Aluminium alloys exhibit typical pure metal texture (Cu-type) on rolling comprising of Cu $\{1\ 1\ 2\} \langle 1\ 1\ 1 \rangle$, brass $\{1\ 1\ 0\} \langle 1\ 1\ 2 \rangle$ and S $\{1\ 2\ 3\} \langle 6\ 3\ 4 \rangle$ orientations, and Cube $\{1\ 0\ 0\} \langle 0\ 0\ 1 \rangle$ and Goss $\{1\ 1\ 0\} \langle 0\ 0\ 1 \rangle$ components were common during annealing [7, 10]. In this aspect an attempt has been made to correlate the tensile properties, formability properties and void coalescence parameters, with texture of sheet metal at different annealing temperatures. The effect of the cube texture on the initiation of localized necking has been studied using numerical methods by Wu et al. [12]. They have inferred that, when a sheet undergoes biaxial tension, ideal cube texture significantly delays the initiation of localized necking [11]. Aluminium alloys exhibit typical pure metal texture (Cu $\{1\ 1\ 2\} \langle 1\ 1\ 1 \rangle$ -type) on rolling comprising of Cu $\{1\ 1\ 2\} \langle 1\ 1\ 1 \rangle$, brass $\{1\ 1\ 0\} \langle 1\ 1\ 2 \rangle$ and S $\{1\ 2\ 3\} \langle 6\ 3\ 4 \rangle$ orientations, and Cube $\{1\ 0\ 0\} \langle 0\ 0\ 1 \rangle$ and Goss $\{1\ 1\ 0\} \langle 0\ 0\ 1 \rangle$ components are common during annealing [10] as seen in **Figure 1**. An Al 8011 aluminium alloy sheet cold-rolled by 95% had a typical fibre texture, which runs from the copper orientation $\{1\ 1\ 2\} \langle 1\ 1\ 1 \rangle$ over the S-orientation $\{1\ 2\ 3\} \langle 6\ 3\ 4 \rangle$ to the brass orientation $\{1\ 1\ 0\} \langle 1\ 1\ 2 \rangle$ in the Euler space. The results were discussed, based on the interaction between precipitation and recrystallization [13, 14]. The cube component recovered quite easily during deformation after large strains as well as during the first step of the annealing treatment, as per the findings of Gerber et al. [15].

Matthies et al. [16] have consolidated all methods of the analysis of texture by pole figure and orientation distribution function (ODF) in Euler space. Knorr et al. [17] and Kocks et al. [18] studied the material property such as strength and deformation behaviour, through texture and failure analysis. Bennett et al. [6] examined the cube $\{1\ 0\ 0\} \langle 0\ 0\ 1 \rangle$ grains before and after stretching and found that there was a translocation. In this aspect this work investigates the mode of evolution of texture components, in commercially available aluminium alloy sheets of three different thicknesses at three different annealing temperatures using numerical modelling practice. The works related to the crystal plastic models are given below. From the results of Al 8011, Al 1145 and Al 1350 alloy, pole figures ODF and alpha-beta fibre, the following discussions were made (**Figure 17**).

11.1 Volume fraction

A plot of the texture component with the annealing temperature for Al 8011 alloy showed a linear relationship for the cube and Goss component. Similarly from **Figures 17** and **18**, cube and RD cube were increasing linearly for Al 1145 alloy. The components S and Cu were in decreasing nature, and a deviation occurred at an annealing temperature of 300°C.

11.2 Al alloy

The evolution of Goss intensity was very negligible in Al 1145 alloy as compared to alloy 8011. The dominant texture component in the annealed microstructure,

that is, cube, was due to the higher nucleation rate of cube grains at the already existing cube bands.

Wu et al. [12] and 1998 have shown that ideal cube texture could lead to sharper yield locus under biaxial stretching and thereby sheet formability. **Figure 18c and d** was clear that the fraction of ideal cube was almost negligible compared to the fraction of cube spread in the microstructure. Apart from the cube component, it was observed that the fractions of RD- and ND-rotated cubes have been enhanced (ND-rotated cube $\{0\ 0\ 1\} \langle 1\ 3\ 0 \rangle$ and RD-rotated cube $\{1\ 3\ 0\} \langle 0\ 0\ 1 \rangle$ were deviated by about 18° along ND and RD, respectively, from the ideal cube orientation). A similar behaviour was observed for the alloy Al 1350.

11.3 Pole figure

From **Figure 17**, the recalculated 111 pole figures with imposed orthotropic sample symmetry could be seen. Here, a gradual diminishing of deformation components can be seen with the simultaneous development of cube texture with annealing temperature for Al 8011 alloy. From **Figure 18**, it can be seen that the difference in elongation along the major and minor axes was significant which implied that the anisotropy was higher in these rolled Al 8011 alloy sheets. **Figures 17 and 18** represent the recalculated 111 pole figures from the ODF with imposed orthotropic sample symmetry for Al 1145 and Al 1350, respectively. It can be seen that significant deformations were retained up to 250°C beyond which cube texture became prominent with increasing annealing temperature.

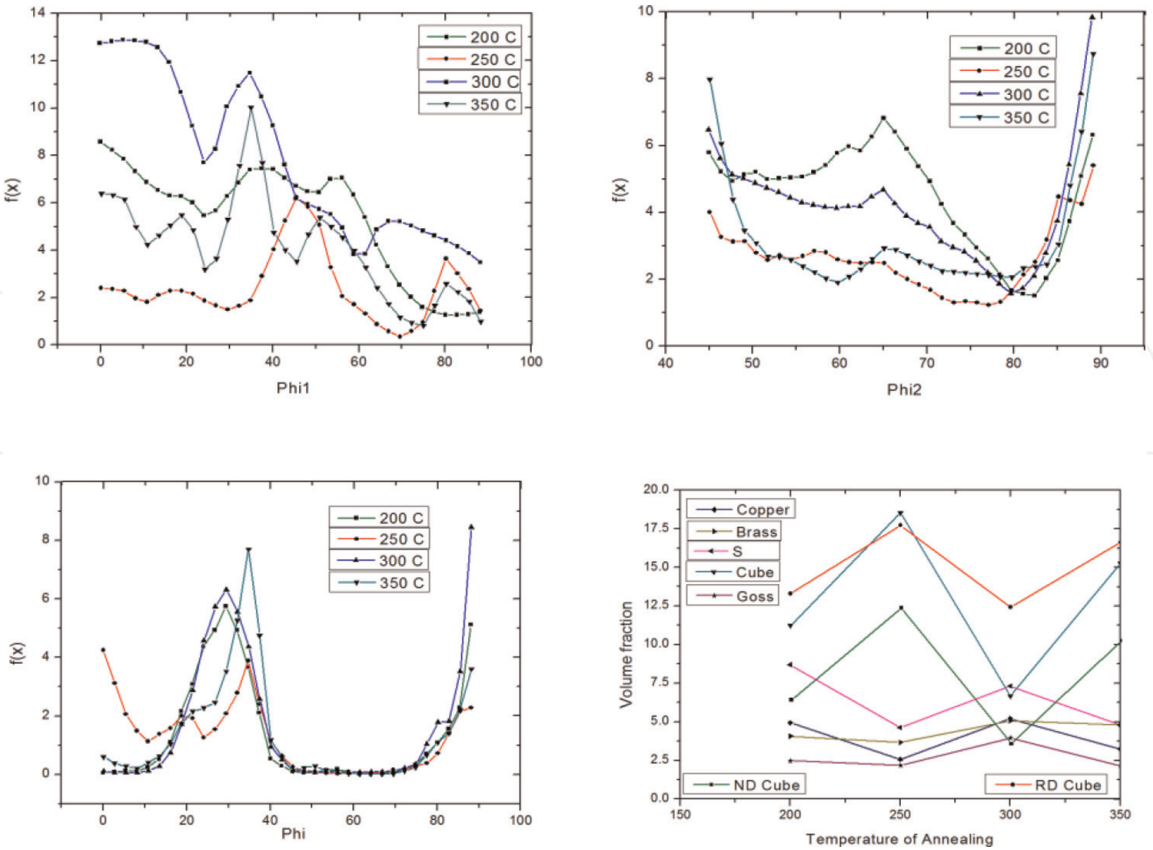


Figure 17. Texture analysis based on ODF for the annealed samples of Al 1350: (a) alpha-fibre, (b) beta-fibre, (c) phi, (d) volume fraction of texture components.

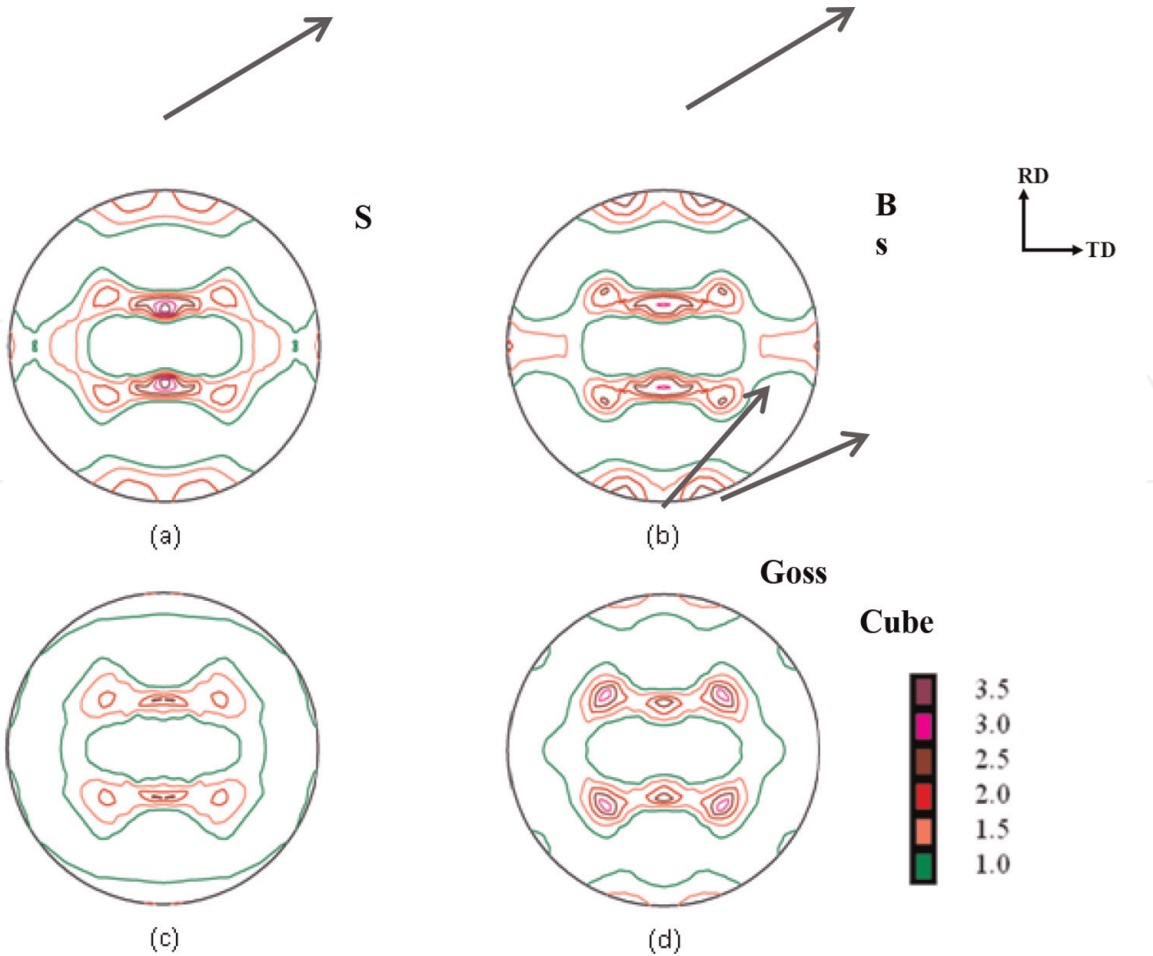


Figure 18.
111 pole figures of annealed samples of Al 8011: (a) 200°C, (b) 250°C, (c) 300°C, (d) 350°C [30, 32–35].

11.4 ODF

The intensity of Cu and S components in the ϕ_2 —45° and ϕ_2 —65° sections, respectively, has decreased with temperature. The ϕ_2 —0° section showed qualitatively the strengthening of cube and Goss intensities as a function of temperature.

11.5 α -Fibre and β -fibre

From the α -fibre, it can be inferred that the Goss components increased with simultaneous fall in the orientation densities ($f(g)$) of deformation components as can be seen from the β -fibre (**Figure 17**) for Al 8011 alloy. The cube orientation showed a strong scattering along the RD in the ϕ_2 —0° section.

Figure 18 showed that the formability in the present set of samples improved with increasing annealing temperature. The presence of precipitates could significantly suppress the cube fraction in the microstructure in turn retaining the deformation components at lower temperatures.

The alpha-fibre plots followed a similar trend in all the cases, particularly at starting ($\phi = 0^\circ$) and end ($\phi = 90^\circ$) locations. As there is an increased annealing temperature, the intensity of alpha-fibre also increases. The trend was different at $\phi_1 = 35^\circ$, where a peak change is observed at all alpha-fibre components. In general, a deep change (intensity of alpha-fibre component) was observed at other annealing temperatures except 300°C. This was due to the equilibrium between precipitation and recrystallization at that temperature. Hence alpha-fibre

component represented 300°C (blue colour) at $\phi_1 = 35^\circ$, $\phi = 45^\circ$ and $\phi_2 = 0^\circ$ shows inconsistent intensity.

Hence these experimental results could not be directly interpreted, but it can be interpreted by fitting these results into the models by simulation approach, which has been discussed in the later part of the section using response surface methodology.

12. FLD using crystal plasticity models

Efforts have been made in recent years to incorporate the plastic anisotropy resulting mainly from a crystallographic texture to the modelling of the deformation of polycrystalline solids [19]. Two types of procedures have been currently being used. The first involved direct crystal plasticity [20], whereas the second represented the yield surface by a closed-form, analytical expression [10, 21]. FLD predictions were compared with the experimental data of annealed aluminium (AA6xxx) sheet. It was found that the Goss orientation $\{0\ 1\ 1\} \langle 1\ 0\ 0 \rangle$ present in the initial texture and the microstructure influenced the formability significantly.

13. Effect of cube texture on sheet metal formability

Wu et al. [12] investigated the effect of the cube texture on the initiation of localized necking, while the ideal cube texture showed decreased formability; for a sheet undergoing biaxial tension, a spread about the cube significantly delayed the initiation of localized necking. The effect of a widespread cube texture on the FLD was path dependent; it decreased the formability for strain paths far away from the equi-biaxial stretching but increased the formability significantly near the equi-biaxial stretching mode. Theoretically, the change in formability near equi-biaxial stretching could be correlated to the sharpness of the yield locus at equi-biaxial tension.

As the annealing temperature increased, the recrystallization and precipitation rates increased [22, 23], which, in turn, resulted in a decrease in time to obtain the conductivity saturating level, and the solute solubility increased resulting in a decrease in the peak conductivity. Creating better texture helped to develop sheet metals with higher formability. By correlation of the parameters, the texture can be optimized. Literatures related to texture optimization have been given.

14. Microstructure and texture versus annealing

Galand et al. [24] have focused on the influence of interconnected Cu microstructure on the electro-migration phenomenon. The microstructure and texture of copper were characterized by electron backscatter diffraction (EBSD). In both cases, no significant differences were observed in terms of the reliability performance versus annealing conditions. On the contrary, a large difference was observed on the electron backscatter diffraction results. Then, a statistical approach was used to investigate local microstructure and texture of copper for 150 nm line width. The results indicated that the morphological parameters of copper can vary with annealing conditions but could lead to similar reliability performances.

It was concluded that these parameters had no relationship with electro-migration phenomena in the interconnects. On the other hand, a high amount of disorientation has been highlighted as responsible for early failures. Also

disorientation resulting in high mean disorientation and high grain boundary densities were the root cause of early failures.

15. Conclusions

This chapter clearly explains the interlinking nature of aluminium and its alloys in terms of its physical size like sheet thickness, annealing temperature, sheet (rolling) orientation, chemical composition versus tensile properties, formability properties, texture properties and void coalescence properties. The desired formability can be seen through the better crystallographic evolution and microstructure or from the fractography void coalescence results. Furthermore investigations could be carried out to prove a well-established strong outcomes in this area.

Acknowledgements

The authors would like to thank our masters, Dr. R. Narayanasamy and Dr. Satyam Suwas, for their input and our beloved daughter V. Suryameena for her support.

Author details


K. Velmanirajan^{1*} and K. Anuradha²

¹ Department of Mechanical Engineering, VSVN Polytechnic College, Virudhunagar, Tamil Nadu, India

² Department of Chemistry, Sri Meenatchi Government Arts College, Madurai, Tamil Nadu, India

*Address all correspondence to: velmanirajan@gmail.com

IntechOpen

© 2019 The Author(s). Licensee IntechOpen. This chapter is distributed under the terms of the Creative Commons Attribution License (<http://creativecommons.org/licenses/by/3.0>), which permits unrestricted use, distribution, and reproduction in any medium, provided the original work is properly cited. 

References

- [1] Narayanasamy R, Parthasarathi NL, Ravindran R, Sathiya Narayanan C. Analysis of fracture limit curves and void coalescence in high strength interstitial free steel sheets formed under different stress conditions. *Materials Science*. 2008;**43**:3351-3363
- [2] Narayanasamy R, Sathiya NC. Some aspects on fracture limit diagram developed for different steel sheets. *Materials Science and Engineering A*. 2006;**417**:197-224
- [3] Xing ZP, Kang SB, Kim HW. Softening behavior of 8011 alloy produced by accumulative roll bonding process. *Scripta Materialia*. 2001;**45**: 597-604
- [4] Takuda H, Yamazaki N, Hatta N, Kikuchi S. Influence of coldrolling and annealing conditions on formability of aluminium alloy sheet. *Journal of Materials Science*. 1995;**30**:957-963
- [5] Kumar A, Satapathy S, Ravi Kumar D. Effect of sheet thickness and punch roughness on formability of sheets in hydromechanical deep drawing. *Journal of Materials Engineering and Performance*. 2010;**19**(8):1150-1160
- [6] Bennett TA, Petrov RH, Kestens LAI. Texture-induced surface roping in an automotive aluminium sheet. *Scripta Materialia*. 2009;**61**(7):733-736
- [7] Engler O, Randle V. *Introduction to Texture Analysis: Macrotexture, Microtexture, and Orientation Mapping*. Second ed. CRC Press; 2009
- [8] Engler O, Lucke K. Mechanisms of recrystallization texture formation in aluminium alloys. *Scripta Metallurgica*. 1992;**27**:1527-1532
- [9] Lademo OG, Pedersen KO, Berstad T, Furub T, Hopperstad OS. An experimental and numerical study on the formability of textured Al-Zn-Mg alloys. *European Journal of Mechanics—A/Solids*. 2008;**27**:116-140
- [10] Lequeu PH, Gilormini P, Montheillet F, Bacroix B, Jonas JJ. Yield surfaces for textured polycrystals—I. Crystallographic approach. *Acta Metallurgica*. 1987;**35**:439
- [11] Crumbach M, Goerdeler M, Gottstein G. Modelling of recrystallisation textures in aluminium alloys II. Model performance and experimental validation. *Acta Materialia*. 2006;**54**:3291-3306
- [12] Wu PD, MacEwen SR, Lloyd DJ, Neale KW. Effect of cube texture on sheet metal formability. *Materials Science and Engineering A*. 2004;**364**: 182-187
- [13] Ryu J-H, Lee DN. The effect of precipitation on the evolution of recrystallization texture in AA8011 aluminum alloy sheet. *Materials Science and Engineering A*. 2002;**336**:225-232
- [14] Lee J-K, Lee DN. Texture control and grain refinement of AA1050 Al alloy sheets by asymmetric rolling. *International Journal of Mechanical Sciences*. 2008;**50**:869-887
- [15] Gerber PH, Tarasiuk J, Th C, Bacroix B. A quantitative analysis of the evolution of texture and stored energy during annealing of cold rolled copper. *Acta Materialia*. 2003;**51**:6359-6371
- [16] Matthies S, Wenk HR, Vinel GW. Some basic concepts of texture analysis and comparison of three methods to calculate orientation distributions from pole figures. *Journal of Applied Crystallography*. 1988;**21**:285-304
- [17] Knorr DB, Peltier JM, Pelloux RM. Influence of Crystallographic texture

and test temperature on initiation and propagation of iodine stress-corrosion cracks in zircaloy. In: *Zirconium in the Nuclear Industry: Sixth International Symposium*. Philadelphia, PA: ASTM; 1972. pp. 627-651

[18] Kocks UF, Tomé CN, Wenk H-R, Mecking H. *Texture and Anisotropy: Preferred Orientations in Polycrystals and their Effects on Materials Properties*. Cambridge University Press; 2000

[19] Ma Q, Mao W, Feng H, Yu Y. Rapid texture measurement of cold-rolled aluminum sheet by X-ray diffraction. *Scripta Materialia*. 2006;**54**:1901-1905

[20] Friedman PA, Pan J. Effects of plastic anisotropy and yield criteria on prediction of forming limit curves. *International Journal of Mechanical Sciences*. 2000;**42**:29-48

[21] Aretz H. Applications of a new plane stress yield function to orthotropic steel and aluminium sheet metals. *Modelling and Simulation in Materials Science and Engineering*. 2004;**12**:491-509

[22] Jining Q, Di Z, Guoding Z, Lee J-C. Effect of temperature on texture formation of 6061 aluminum sheet in equal channel angular pressing. *Materials Science and Engineering A*. 2005;**408**:79-84

[23] Aghaie-Khafri M, Mahmudi R. Optimizing homogenization parameters for better stretch formability in an Al-Mn-Mg alloy sheet. *Materials Science and Engineering A*. 2005;**399**:173-180

[24] Galand R, Haxaire K, Arnaud L, Petitprez E, Clement L, Waltz P, et al. Microstructure and texture analysis of narrow copper line versus widths and annealing for reliability improvement. *Microelectronic Engineering*. 2011;**88**: 661-665

[25] Kim J, Gao X, Srivatsan TS. Modelling of crack growth in ductile

solids: A three-dimensional analysis. *International Journal of Solids and Structures*. 2003;**40**:7357-7374

[26] Narayanasamy R, Ravindran R, Manonmani K. An analysis of void coalescence in AL 5052 alloy sheets annealed at different temperature formed under different stress conditions. *Materials Science and Engineering A*. 2009;**507**:252-267

[27] Ravikumar D, Swaminathan K. Formability of two aluminium alloys. *Materials Science and Technology*. 1999; **15**:1241-1252

[28] Kristensson O. Numerically produced forming limit diagrams for metal sheets with voids considering micromechanical effects. *European Journal of Mechanics—A/Solids*. 2006; **25**:13-23

[29] Son H-S, Kim Y-S, Na K-H, Hwang S-M. Effect of void shape and its growth on forming limits for anisotropic sheets containing non-spherical voids. *ASME: The American Society of Mechanical Engineers*. 2004;**47**:512-520

[30] Velmanirajan K, Thaheer ASA, Narayanasamy R, Basha CA. Numerical modelling of aluminium sheets formability using response surface methodology. *Materials & Design*. 2012; **41**:239-254. DOI: doi.org/10.1016/j.matdes.2012.05.027

[31] Chandra Sekhar K, Narayanasamy R, Velmanirajan K. Experimental investigations on microstructure and formability of cryorolled AA 5052 sheets. *Materials & Design*. 2014;**53**: 1064-1070. DOI: [10.1016/j.matdes.2013.08.008](http://doi.org/10.1016/j.matdes.2013.08.008)

[32] Velmanirajan K, Anuradha K, Thaheer ASA, Narayanasamy R, Madhavan R, Suwas S. Experimental investigation of forming limit, void coalescence and crystallographic textures of aluminum alloy 8011 sheet

annealed at various temperatures.
Archives of Civil and Mechanical
Engineering. 2014a;**14**(3):398-416

[33] Velmanirajan K, Anuradha K,
Thaheer ASA, Ponalagusamy R,
Narayanasamy R. Statistical evaluation
of forming limit diagram for annealed
Al 1350 alloy sheets using first order
reliability method. Applied
Mathematical Modeling. 2014b;**38**(1):
145-167

[34] Velmanirajan K, Thaheer ASA,
Narayanasamy R. Effect of annealing
temperature in Al 1145 alloy sheets on
formability void coalescence and texture
analysis. Journal of Materials
Engineering and Performance. 2013;
22(4):1091-1107

[35] Velmanirajan K, Narayanasamy R,
Anuradha K. Effect of chemical
composition on texture using response
surface methodology. Journal of
Materials Engineering and Performance.
2013;**22**(11):3237-3257